IAC-12-C1.2.9

GLOBAL LOW-THRUST GUIDANCE SCHEME FOR DISAGGREGATED SPACECRAFT ARCHITECTURES

L. Mazal
Distributed Space Systems Lab, Faculty of Aerospace Engineering, Technion–Israel Institute of Technology, Haifa 32000, Israel; leomazal@techunix.technion.ac.il

G. Mingotti[1], P. Gurfil[2]

The main idea of disaggregated satellites is to distribute the functionality of a single monolithic satellite among multiple physically-independent wireless-communicating modules. These new architectures raises the emerging concept of cluster flight, in which the distance between any two modules of the cluster must be kept between prescribed upper and lower thresholds. This work is concerned with strategies to efficiently perform cluster-establishment. The main goal of the establishment is to deploy the modules in such a manner that the necessity of future corrective maneuvers, after the establishment, is reduced as much as possible. To that end, the establishment maneuver steers the cluster to relative initial conditions, which are favorable to avoid distance drifts, as well as enable the payload module, to track a prescribed reference trajectory. A cooperative guidance law, for cluster establishment and re-establishment, is proposed. As the modules are assumed to be equipped with low-thrust chemical (cold-gas) propulsion systems, thrust of type bang-off-bang thrust is considered, as well as perturbations due to the Earth oblateness and drag.

I. INTRODUCTION

In disaggregated space architectures (DSA), the main idea is to replace monolithic satellites by multiple free-flying modules interacting through wireless cross-links. These disaggregated satellite modules (DSM) are heterogeneous, having one or more pre-determined functions, e.g. navigation, attitude control, power generation and payload operation. DSA enable extended spacecraft operability; for instance, a failed DSM can be replaced, whereas in a monolithic satellite a failed subsystem might cause premature mission termination.

Unlike satellite formation flying missions, the DSM do not have to operate in a tightly-controlled formation; instead, they are required to maintain the inter-module distances bounded for the entire mission lifetime. This concept is termed *cluster flight*. Some of the main ideas on which DSA rely upon were formally introduced by Brown and Eremenko[1]. Later works discussed the advantages and disadvantages of DSA compared to conventional architectures[2].

Cluster flight is challenging, because without control forces initially-close DSM will tend to drift apart due to differential accelerations. Since the total propellant on each DSM is strictly limited, and the propulsion system is of limited performance (e.g. cold-gas), keeping a cluster of DSM in prescribed maximum and minimum distances while maintaining at least one of the DSM (e.g., the payload module) on a given reference orbit becomes an extremely challenging problem. This problem couples high-fidelity astrodynamical modeling, guidance, and orbit control.

[1]Distributed Space Systems Lab, Faculty of Aerospace Engineering, Technion–Israel Institute of Technology, Haifa 32000, Israel; mingotti@technix.technion.ac.il
[2]Distributed Space Systems Lab, Faculty of Aerospace Engineering, Technion–Israel Institute of Technology, Haifa 32000, Israel; pgurfil@technion.ac.il

The most significant perturbations affecting low Earth-orbit satellites are the Earth oblateness and drag. Many works presented strategies for mitigating the relative drifts among satellites subject to the main perturbations. Constraints leading to J_2 secular effect mitigation and concomitant optimal multi-impulsive maneuvers for spacecraft formation flying were proposed[3, 4, 5, 6]. A recent extension of perturbation mitigation for the problem of cluster flight was proposed[7].

A critical fact to consider concerns the ballistic coefficients of the DSM. In the presence of drag, differences in ballistic coefficients may cause rapid drift among the DSM. Consequently, any cluster-keeping strategy should consider balancing the ballistic coefficients after any maneuver.

Impulsive velocity changes, while frequently providing useful approximations, do not represent realistic maneuvers, which are continuous processes that last at least a few seconds. In this context, several works dealt with time-continuous maneuvers for distributed space systems. Most of these works derived control laws with a continuously-variable thrust magnitude[8, 9, 10]. Moreover, the issue of different resulting masses was neglected; however, this issue is crucial for cluster flight. Cold-gas propulsion systems are useful for disaggregated spacecraft due to simplicity and low cost. However, a significant drawback is that the magnitude of the exerted thrust cannot be regulated. This feature leads to control profiles known as bang-off-bang. Attempts at finding optimal trajectories for satellites, while assuming constant thrust levels, were previously made[11, 12].

In Ref. [13], cooperative optimal guidance laws for cluster-establishment were derived. This guidance scheme considered bang-off-bang thrust profiles. The assumed dynamical model included drag and the first term of the zonal harmonic geopotential, J_2. In this work, those guidance laws are reviewed and assessed in more complete astrodynamical scenarios, including other, so far unconsidered, perturbations.

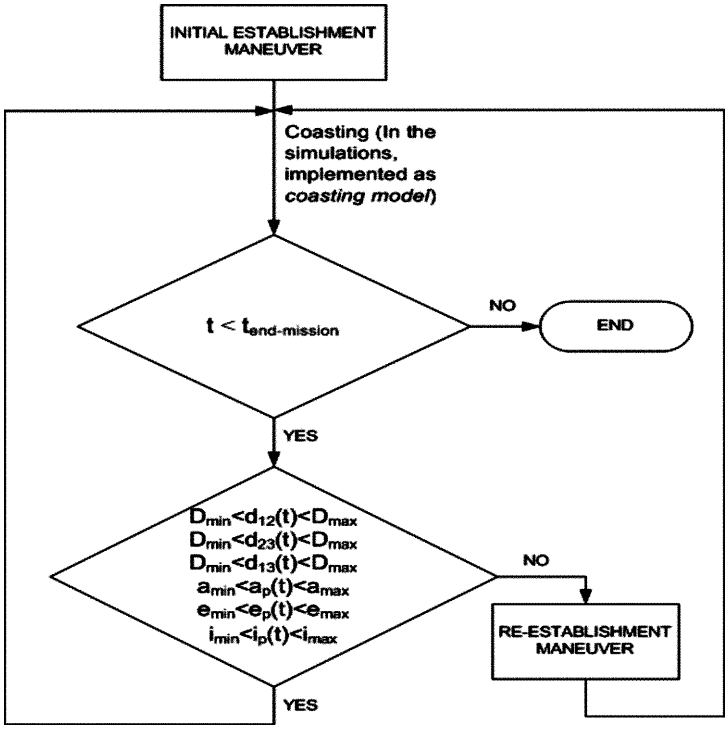

Fig. 1: Flowchart of the global cluster-keeping scheme.

The followed approach steers the DSM, from given initial conditions, to terminal conditions that mitigate the relative drifts while keeping the ballistic coefficients balanced. Based on these maneuvers, a global strategy to hold the cluster for long-time scales is proposed.

In the examples shown in Ref. [13], it was observed that, after the maneuvers, the distances between DSM might secularly increase or decrease. However, for collision avoidance, it is preferable an increasing secular behavior of the post-maneuvers distances. This work provides an insight on how to obtain an increasing secular behavior rather than a decreasing one, for this type of maneuvers.

II. GLOBAL STRATEGY

Consider a cluster of 3 modules. It is required, at every time t, to hold the distances between any two modules $d_{ij}(t)\ i,j = 1,2,3$ between a lower and an upper threshold, $D_{\min}$ and $D_{\max}$ respectively. The distance between modules i and j is given by

$$d_{ij}(t) \triangleq \|\mathbf{r}_i(t) - \mathbf{r}_j(t)\| \tag{1}$$

where $\mathbf{r}_i$ and $\mathbf{r}_j$ represent the position vectors of modules i and j respectively. Moreover, additional constraints may be posed on the payload orbit, by requiring

$$\begin{aligned} a_{\min} \leq a_p(t) \leq a_{\max} \\ e_{\min} \leq e_p(t) \leq e_{\max} \\ i_{\min} \leq i_p(t) \leq i_{\max} \end{aligned} \tag{2}$$

where a represents the semimajor axis, e is the eccentricity, and i is the inclination. The sub-index $(\cdot)_p$ denotes the orbital element $(\cdot)$ referred to the payload, and the sub-indices $(\cdot)_{\min}$ and $(\cdot)_{\max}$ denote lower and upper thresholds respectively, for the corresponding orbital element $(\cdot)$.

The global strategy described in this work consists of performing a cooperative establishment maneuver at the beginning of the mission, and performing further cooperative re-establishment maneuvers at any later time upon necessity. By necessity, it is meant that, at time t, any of the constraints on $d_{ij}(t)\ i,j = 1,2,3$ or those given by (2) exceeds the prescribed thresholds. The flowchart in Fig. 1 illustrates the idea, where $t_{\text{end-mission}}$ denotes the final time of the entire mission. In light of the mentioned strategy, it is important that each establishment (or re-establishment) maneuver steers the system to a set of states that enable the system to remain as long as possible between the given thresholds, so that to reduce the number of required maneuvers along the mission lifetime. The states attained at the end of the maneuver are denominated as terminal states. The maneuvers proposed in this work are aimed at reaching specific terminal constraints, which already proved to be efficient in terms of allowing long time intervals before the next corrective maneuver[7, 13]. While in Ref. [7] the maneuvers were assumed to be impulsive, in Ref. [13] were assumed to last a finite time. In the latter work, the maneuvers were derived assuming a specific dynamic model. However, as any assumed dynamical model is limited, it differs from a real scenario in which unconsidered perturbation will certainly affect the system. In Ref. [13], the derived maneuvers were assessed in the same dynamical model used as design model, but not in more realistic environments including perturbations not considered in the design model. Hence, the main goal of this work is to examine the execution of those maneuvers in more realistic scenarios, in which some unconsidered astrodynamical effects as well as possible measurement errors take place.

The criterion utilized to qualify the success of the maneuver is observing the long-term behavior of the cluster after the maneuver. Roughly speaking, the longer the cluster modules coast with no need of a re-establishment maneuver, the more efficient the maneuver was. To model the coasting of the modules, an astrodynamical model including geopotential accelerations up to degree and order 21, drag, solar radiation pressure, and third body effects was implemented. For the upcoming explanations, this model is called *coasting model*.

III. COOPERATIVE OPTIMAL ESTABLISHMENT

This section reviews the cooperative establishment maneuvers aimed at targeting specific constraints on the terminal states of the cluster [13]. These constraints mitigate in a significant manner the secular drift of the distances between any two modules of the cluster.

Each module is equipped with four equal thrusters, with a constant thrust magnitude T_n, i.e. the operation profile for each thruster is bang-off-bang. The engines are disposed as two pair of opposed thrusters, and the axes of the two pairs are orthogonal.

In order to facilitate the mathematical formulation of the optimal guidance problem, an artificial *dual-engine* configuration is utilized. It assumes that only one of the four engines is used to thrust. It leads to the following expression for the control thrust, of module k ($k = 1, 2, 3$), in an Earth Centered Inertial (ECI) frame [13]:

$$\mathbf{T}_k = \sigma_k \, T_n \begin{bmatrix} \cos(\alpha_k)\cos(\delta_k) \\ \sin(\alpha_k)\cos(\delta_k) \\ \sin(\delta_k) \end{bmatrix} \tag{3}$$

where σ_k represents the throttle parameter (which for the correct solution must be either 0 or 1), and α_k and δ_k denote azimuth and declination angles respectively, all corresponding to the module k.

On the other hand, the *dual-engine* configuration assumes that the pair of thrusters orthogonal to Engine 1, is used to intentionally dispose mass in case of necessity. The necessity of intentionally dispose slight amount of mass might arise due to constraints imposed on the terminal masses of the modules [13]. Therefore, the total mass consumption is given by

$$\dot{m}_k = -\sigma_k \, \frac{T_n}{I_{sp}\, g_0} - \gamma_k \, \frac{2T_n}{I_{sp}\, g_0} \tag{4}$$

where γ_k represents a throttle parameter regulating the intentional mass disposal of module k, which for the correct solution must be either 0 or 1. I_{sp} represents the specific impulse and g_0 denotes the gravitational acceleration at sea level.

Define the ECI frame, with its fundamental plane lying on the equatorial plane, its $\hat{x}$ axis pointing towards the vernal equinox, its $\hat{z}$ axis pointing towards the geographic north pole, and the $\hat{y} \triangleq \hat{z} \times \hat{x}$. In this frame, $\mathbf{r}_k \triangleq [x_k \; y_k \; z_k]^\top$ and $\mathbf{v}_k \triangleq [vx_k \; vy_k \; vz_k]^\top = [\dot{x}_k \; \dot{y}_k \; \dot{z}_k]^\top$ respectively denote the position and velocity vectors of module k.

The main goal of the maneuvers herein developed is to attain, at the end of the maneuver $t = t_f$, terminal states that hold

$$\begin{aligned} \mathbf{r}_2(t_f) =& \mathcal{R}(\Delta\Omega_{12}) \left[\mathbf{r}_1(t_f) + \mathbf{v}_1(t_f)\, \Delta t_{12} - \frac{\mu}{2} \frac{\mathbf{r}_1(t_f)}{\|\mathbf{r}_1(t_f)\|^3} \, \Delta t_{12}^2 \right] \\ \mathbf{v}_2(t_f) =& \mathcal{R}(\Delta\Omega_{12}) \left[\mathbf{v}_1(t_f) - \mu \frac{\mathbf{r}_1(t_f)}{\|\mathbf{r}_1(t_f)\|^3} \, \Delta t_{12} \right] \end{aligned} \tag{5}$$

$$\begin{aligned} \mathbf{r}_3(t_f) =& \mathcal{R}(\Delta\Omega_{13}) \left[\mathbf{r}_1(t_f) + \mathbf{v}_1(t_f)\, \Delta t_{13} - \frac{\mu}{2} \frac{\mathbf{r}_1(t_f)}{\|\mathbf{r}_1(t_f)\|^3} \, \Delta t_{13}^2 \right] \\ \mathbf{v}_3(t_f) =& \mathcal{R}(\Delta\Omega_{13}) \left[\mathbf{v}_1(t_f) - \mu \frac{\mathbf{r}_1(t_f)}{\|\mathbf{r}_1(t_f)\|^3} \, \Delta t_{13} \right] \end{aligned} \tag{6}$$

where

$$\mathcal{R}(\Delta\Omega_{1p}) \triangleq \begin{bmatrix} +\cos(\Delta\Omega_{1p}) & \sin(\Delta\Omega_{1p}) & 0 \\ -\sin(\Delta\Omega_{1p}) & \cos(\Delta\Omega_{1p}) & 0 \\ 0 & 0 & 1 \end{bmatrix} \tag{7}$$

$p = 2, 3$.

In addition, in order to avoid differences in the ballistic coefficients assuming constant cross-sectional area and drag coefficient, it is also required that

$$m_1(t_f) = m_2(t_f) \tag{8}$$

$$m_1(t_f) = m_3(t_f) \tag{9}$$

Constraints for the terminal states of the payload can be set as

$$\begin{aligned} a_1(t_f) =& -\frac{\mu \, \|\mathbf{r}_1(t_f)\|}{\|\mathbf{v}_1(t_f)\|^2 \, \|\mathbf{r}_1(t_f)\| - 2\mu} = a_{\mathcal{D}} \\ e_1(t_f) =& \sqrt{1 + \frac{\|\mathbf{r}_1(t_f) \times \mathbf{v}_1(t_f)\|^2}{\mu^2 \, \|\mathbf{r}_1(t_f)\|} \left(\|\mathbf{v}_1(t_f)\|^2 \, \|\mathbf{r}_1(t_f)\| - 2\mu \right)} = e_{\mathcal{D}} \\ i_1(t_f) =& \arccos\left(\frac{x_1(t_f)\, vy_1(t_f) - y_1(t_f)\, vx_1(t_f)}{\|\mathbf{r}_1(t_f) \times \mathbf{v}_1(t_f)\|} \right) = i_{\mathcal{D}} \end{aligned} \tag{10}$$

which enable the payload of the cluster to track a reference orbit given by a desired semimajor axis $a_{\mathcal{D}}$, eccentricity $e_{\mathcal{D}}$, and inclination $i_{\mathcal{D}}$.

To derive a cooperative optimal guidance law, a cost function aimed at reducing the fuel consumption was set as

$$\mathcal{J} = \int_{t_i}^{t_f} \sum_{k=1}^{3} \left(\sigma_k \, T_n + 2\, \gamma_k \, T_n \right) \, \mathrm{dt} \tag{11}$$

where t_i is the initial time of the maneuver.

Assuming that the modules have equal and constant cross-sectional areas and drag coefficients, the dynamical model considered to design the maneuvers was given by

$$\begin{aligned} \dot{\mathbf{r}}_k =& \mathbf{v}_k \\ \dot{\mathbf{v}}_k =& -\mu \frac{\mathbf{r}_k}{\|\mathbf{r}_k\|^3} - \frac{\mu \, J_2 \, R_q^2}{2 \, \|\mathbf{r}_k\|^5} \left(6 \begin{bmatrix} 0 \\ 0 \\ z_k \end{bmatrix} + \left[3 - 15 \left(\frac{z_k}{\|\mathbf{r}_k\|} \right)^2 \right] \mathbf{r}_k \right) \\ & - \rho \, \|\mathbf{v}_k\| \, \frac{S \, C_D}{2 \, m_k} \mathbf{v}_k + \frac{\mathbf{T}_k}{m_k} \\ \dot{m}_k =& -\sigma_k \, \frac{C_k}{I_{sp}\, g_0} - \gamma_k \, \frac{D_k}{I_{sp}\, g_0} \end{aligned} \tag{12}$$

which represents Keplerian dynamics perturbed by the first term of the zonal harmonics potential, drag and thrust. m_k denotes the instantaneous mass of the satellite k. Moreover, the density ρ was considered constant.

According to optimal control theory [14, 15], the Hamiltonian of the problem is defined as

$$\begin{aligned}\mathcal{H} = &+ \sigma_1 T_n + \sigma_2 T_n + \sigma_3 T_n + 2\gamma_1 T_n + 2\gamma_2 T_n + 2\gamma_3 T_n \\ &+ \boldsymbol{\lambda_{r_1}}^\top \mathbf{v}_1 + \boldsymbol{\lambda_{r_2}}^\top \mathbf{v}_2 + \boldsymbol{\lambda_{r_3}}^\top \mathbf{v}_3 + \boldsymbol{\lambda_{v_1}}^\top \dot{\mathbf{v}}_1 + \boldsymbol{\lambda_{v_2}}^\top \dot{\mathbf{v}}_2 \\ &+ \boldsymbol{\lambda_{v_3}}^\top \dot{\mathbf{v}}_3 - \lambda_{m_1} \left(\sigma_1 \frac{T_n}{I_{sp}\, g_0} + \gamma_1 \frac{2T_n}{I_{sp}\, g_0} \right) \\ &- \lambda_{m_2} \left(\sigma_2 \frac{T_n}{I_{sp}\, g_0} + \gamma_2 \frac{2T_n}{I_{sp}\, g_0} \right) \\ &- \lambda_{m_3} \left(\sigma_3 \frac{T_n}{I_{sp}\, g_0} + \gamma_3 \frac{2T_n}{I_{sp}\, g_0} \right)\end{aligned} \tag{13}$$

where $\boldsymbol{\lambda}_{\mathbf{r}_k}$, $\boldsymbol{\lambda}_{\mathbf{v}_k}$, and λ_{m_k} are the co-states, corresponding to $\mathbf{r}_k$, $\mathbf{v}_k$ and m_k, respectively.

The dynamics of the co-states are given by

$$\begin{aligned}\dot{\boldsymbol{\lambda}}_{r_k} &= -\left[\frac{\partial \mathcal{H}}{\partial \mathbf{r}_k}\right]^\top \\ \dot{\boldsymbol{\lambda}}_{v_k} &= -\left[\frac{\partial \mathcal{H}}{\partial \mathbf{v}_k}\right]^\top \\ \dot{\lambda}_{m_k} &= -\frac{\partial \mathcal{H}}{\partial m_k}\end{aligned} \tag{14}$$

The Hamiltonian of Eq. (13) can be written as $\mathcal{H} = \mathcal{H}_1 + \mathcal{H}_2 + \mathcal{H}_3$, where

$$\begin{aligned}\mathcal{H}_k = &\sigma_k T_n + 2\gamma_k T_n + \boldsymbol{\lambda_{r_k}}^T \mathbf{v}_k + \boldsymbol{\lambda_{v_k}}^T \dot{\mathbf{v}}_k \\ &- \lambda_{m_k} \left(\sigma_k \frac{T_n}{I_{sp}\, g_0} + \gamma_k \frac{2T_n}{I_{sp}\, g_0} \right)\end{aligned} \tag{15}$$

and $\mathcal{H}_k$ can be re-written as $\mathcal{H}_k = \hat{\mathcal{H}}_k + \bar{\mathcal{H}}_k$, where $\hat{\mathcal{H}}_k$ denotes the sum of the terms depending on the control variables, and $\bar{\mathcal{H}}_k$ denotes the sum of the terms independent of the control variables. Introducing the corresponding expressions for $\dot{\mathbf{v}}_k$ from Eqs. (12), and defining $\boldsymbol{\lambda}_{\mathbf{v}_k} \triangleq [\lambda_{vx_k},\, \lambda_{vy_k},\, \lambda_{vz_k}]^\top$, the following expression is obtained:

$$\begin{aligned}\hat{\mathcal{H}}_k = &+\sigma_k \left(T_n + \frac{T_n}{m_k} \tilde{\mathcal{H}}_k - \lambda_{m_k} \frac{T_n}{I_{sp}\, g_0} \right) \\ &+\gamma_k \left(2T_n - \lambda_{m_k} \frac{2T_n}{I_{sp}\, g_0} \right)\end{aligned} \tag{16}$$

where

$$\begin{aligned}\tilde{\mathcal{H}}_k = &\lambda_{vx_k} \cos(\alpha_k) \cos(\delta_k) + \lambda_{vy_k} \sin(\alpha_k) \cos(\delta_k) \\ &+ \lambda_{vz_k} \sin(\delta_k)\end{aligned} \tag{17}$$

For each k, Eq. (16) will be utilized to minimize the total Hamiltonian $\mathcal{H}$, as a function of $(\sigma_k,\, \alpha_k,\, \delta_k,\, \gamma_k)$. Notice that even though σ_k and γ_k can only be 0 or 1 (according to the bang-off-bang profile of the engines), for the optimal control problem statement, they are assumed to belong to $\sigma_k \in [0,\, 1]$ and $\gamma_k \in [0,\, 1]$. The optimal solution will set them as 0 or 1. The global minimum of $\hat{\mathcal{H}}_k$ is found either at

$$\begin{cases} \alpha_k^{1*} = \arctan\left(\dfrac{\lambda_{vy_k}}{\lambda_{vx_k}} \right) \\ \delta_k^{1*} = \arctan\left(\dfrac{\lambda_{vz_k}}{\lambda_{vx_k} \cos\alpha_k^* + \lambda_{vy_k} \sin\alpha_k^*} \right) \end{cases} \tag{18}$$

or at

$$\begin{cases} \alpha_k^{2*} = \alpha_k^{1*} + \pi \\ \delta_k^{2*} = -\delta_k^{1*} \end{cases} \tag{19}$$

$\tilde{\mathcal{H}}_k$ is computed at both two solution candidates given by Eq. (18) and Eq. (19); the candidate that yields the lowest $\tilde{\mathcal{H}}_k$ allows to choose the optimal set of α_k^* and δ_k^*. If $\lambda_{vx_k} = \lambda_{vy_k} = 0$ for some t, α_k is irrelevant and $\delta_k = -\text{sign}(\lambda_{vz_k})\pi/2$.

Define the switching functions S_{σ_k} as

$$S_{\sigma_k} \triangleq \left(T_n + \frac{T_n}{m_k} \tilde{\mathcal{H}}_k - \lambda_{m_k} \frac{T_n}{I_{sp}\, g_0} \right) \tag{20}$$

Then,

$$\sigma_k^* = \begin{cases} 1, \text{ if } S_{\sigma_k} < 0, \\ 0, \text{ if } S_{\sigma_k} \geq 0 \end{cases} \tag{21}$$

Similarly, define the switching functions S_{γ_k} as

$$S_{\gamma_k} \triangleq 2T_n - \lambda_{m_k} \frac{2T_n}{I_{sp}\, g_0} \tag{22}$$

so γ_k is given by

$$\gamma_k^* = \begin{cases} 1, \text{ if } S_{\gamma_k} < 0, \\ 0, \text{ if } S_{\gamma_k} \geq 0 \end{cases} \tag{23}$$

Finally, $(\alpha_k^*,\, \sigma_k^*,\, \delta_k^*,\, \delta_k^*)$ is the argument that globally minimizes $\mathcal{H}_k$, and therefore the total $\mathcal{H}$.

In order to obtain the terminal constraints for the co-states, the function Φ is defined as

$$\begin{aligned}\Phi = &+ \nu_1 \left(-\frac{\mu \left\| \mathbf{r}_1(t_f) \right\|}{\left\| \mathbf{v}_1(t_f) \right\|^2 \left\| \mathbf{r}_1(t_f) \right\| - 2\mu} - a_{\mathcal{D}} \right) \\ &+ \nu_2\, \Psi_e \\ &+ \nu_3 \left(\arccos\left(\frac{x_1(t_f)\, vy_1(t_f) - y_1(t_f)\, vx_1(t_f)}{\left\| \mathbf{r}_1(t_f) \times \mathbf{v}_1(t_f) \right\|} \right) - i_{\mathcal{D}} \right) \\ &+ [\nu_4\ \nu_5\ \nu_6]\, \Psi_{\mathbf{r}_2} \\ &+ [\nu_7\ \nu_8\ \nu_9]\, \Psi_{\mathbf{v}_2} \\ &+ [\nu_{10}\ \nu_{11}\ \nu_{12}]\, \Psi_{\mathbf{r}_3} \\ &+ [\nu_{13}\ \nu_{14}\ \nu_{15}]\, \Psi_{\mathbf{v}_3} \\ &+ \nu_{16} \left(m_2(t_f) - m_1(t_f) \right) \\ &+ \nu_{17} \left(m_3(t_f) - m_1(t_f) \right)\end{aligned} \tag{24}$$

where

$$\begin{aligned}\Psi_e \triangleq &\sqrt{1 + \frac{\left\| \mathbf{r}_1(t_f) \times \mathbf{v}_1(t_f) \right\|^2}{\mu^2 \left\| \mathbf{r}_1(t_f) \right\|} \left(\left\| \mathbf{v}_1(t_f) \right\|^2 \left\| \mathbf{r}_1(t_f) \right\| - 2\mu \right)} \\ &- e_{\mathcal{D}}\end{aligned} \tag{25}$$

$$\begin{aligned}\Psi_{\mathbf{r}_2} \triangleq &\mathcal{R}(\Delta\Omega_{12}) \left[\mathbf{r}_1(t_f) + \mathbf{v}_1(t_f)\, \Delta t_{12} - \frac{\mu}{2} \frac{\mathbf{r}_1(t_f)}{\left\| \mathbf{r}_1(t_f) \right\|^3} \Delta t_{12}^2 \right] \\ &- \mathbf{r}_2(t_f)\end{aligned} \tag{26}$$

$$\begin{aligned}\Psi_{\mathbf{v}_2} \triangleq &\mathcal{R}(\Delta\Omega_{12}) \left[\mathbf{v}_1(t_f) - \mu \frac{\mathbf{r}_1(t_f)}{\left\| \mathbf{r}_1(t_f) \right\|^3} \Delta t_{12} \right] \\ &- \mathbf{v}_2(t_f)\end{aligned} \tag{27}$$

$$\begin{aligned}\Psi_{\mathbf{r}_3} \triangleq &\mathcal{R}(\Delta\Omega_{13}) \left[\mathbf{r}_1(t_f) + \mathbf{v}_1(t_f)\, \Delta t_{13} - \frac{\mu}{2} \frac{\mathbf{r}_1(t_f)}{\left\| \mathbf{r}_1(t_f) \right\|^3} \Delta t_{13}^2 \right] \\ &- \mathbf{r}_3(t_f)\end{aligned} \tag{28}$$

$$\Psi_{\mathbf{v}_3} \triangleq \mathcal{R}(\Delta\Omega_{13}) \left[\mathbf{v}_1(t_f) - \mu \frac{\mathbf{r}_1(t_f)}{\|\mathbf{r}_1(t_f)\|^3} \Delta t_{13} \right] - \mathbf{v}_3(t_f) \tag{29}$$

Then, it follows that

$$\begin{aligned} \boldsymbol{\lambda}_{\mathbf{r}_k}(t_f) &= \left[\frac{\partial \Phi}{\partial \mathbf{r}_k(t_f)} \right]^\top \\ \boldsymbol{\lambda}_{\mathbf{v}_k}(t_f) &= \left[\frac{\partial \Phi}{\partial \mathbf{v}_k(t_f)} \right]^\top \\ \boldsymbol{\lambda}_{m_k}(t_f) &= \left[\frac{\partial \Phi}{\partial m_k(t_f)} \right]^\top \end{aligned} \tag{30}$$

III.I Two-Point Boundary Value Problem

Eqs. (12) and Eqs. (14) constitute a set of 42 ordinary differential equations, whose boundary conditions are given by the initial conditions and Eqs. (30). Along with the set of unknowns ν_j, $(j = 1, 2, \ldots, 17)$ and the terminal constraints (5)-(10), this two-point boundary value problem is highly non-linear and thus should be numerically solved. To that end, a Matlab® routine, called *bvp4c*®, which is based on collocation methods, is utilized. However, due to the discontinuous behavior of σ_k and γ_k is not possible to obtain a solution from the numerical solver, as it was designed for continuous dynamical systems. In order to implement the binary control laws for σ_k and γ_k as smooth functions, amenable for the numerical processing, Eq. (21) is replaced by

$$\sigma_k = -\frac{\arctan(q_\sigma \, S_{\sigma_k}) + \pi/2}{\pi} + 1 \tag{31}$$

and Eq. (23) by

$$\gamma_k = -\frac{\arctan(q_\gamma \, S_{\gamma_k}) + \pi/2}{\pi} + 1 \tag{32}$$

where q_σ and q_γ are parameters utilized to perform a continuation process to numerically solve the two-point boundary value problem. As q_σ tends to infinity, Eq. (31) tends to the corresponding binary function, in the same manner as Eq. (32) does for $q_\gamma \longrightarrow \infty$. The numerical solver *bvp4c*® relies on initial guesses for the whole solution. Hence, to obtain a good initial guess, it is necessary to start with low values (order of magnitude of 1) of q_σ and q_γ, and then the obtained solution is used as the next initial guess for the next run, where q_σ and q_γ are both increased by an order of magnitude. The process is iteratively continued until high enough values of q_σ and q_γ are reached, such that the obtained thrust profile is bang-off-bang. At orders of magnitude of 10^4, the thrust profile is already perceived as bang-off-bang.

III.II Assessing the guidance laws

The guidance law resulting from solving the two-boundary value problem described in Section III. represents an open-loop control law. For every set of initial states $\mathbf{Y}(t_i)$ and a terminal time t_f, the solution of the two-boundary value problem is the optimal guidance vector given as a function of time.

$$\mathbf{u}(t; \mathbf{Y}(t_i), t_f) \triangleq (\alpha_k^*(t), \, \delta_k^*(t), \, \sigma_k^*(t), \, \gamma_k^*(t)) \tag{33}$$

In real scenarios there exist astrodynamical forces which have been not considered in the design dynamical model given in Eq. (12). Hence, if the cluster is steered according to (33), it is expected that at the end of the maneuver the actual terminal states will be different from the design values. Consequently, the constraints (5), (6) would be not satisfied. On the other hand, the constraints (8) and (9) will be satisfied as long as the thrusters are fired according to $\sigma_k^*(t)$ and $\gamma_k^*(t)$. The aforementioned effects may affect the long term performances of the establishment maneuvers. It is then, mandatory to evaluate the long term behavior of the cluster resulting from executing the maneuvers in a more realistic environment.

Generally speaking, in maneuver design, if the design model is far from the real scenario, open-loop guidance laws should be implemented in a closed-loop scheme. In other words, it is desired to execute the control commands as functions of the actual state rather than as functions of time, so the steering system is capable of coping with unconsidered perturbations.

The guidance law was tested in an open-loop scheme, as well as in an *artificially* closed-loop method. The guidance law $\mathbf{u}(t; \mathbf{Y}(t_i), t_f)$ derived for a given set of initial conditions $\mathbf{Y}(t_i)$ and a terminal time t_f, can be implemented in a closed-loop scheme by recomputing, at any time $t = \tau$, a new guidance law

$$\mathbf{u}(t; \mathbf{Y}(\tau), t_f - \tau) \tag{34}$$

The frequency at which it is recomputed depends on the capabilities of the system, but the higher the frequency the more similar to a real closed-loop control scheme.

Every time the maneuver was recomputed, measurements errors were modeled and added to the real states, representing that the satellite is fed-back with measurements instead of real states. Hence, the state input $\hat{\mathbf{Y}}(\tau)$ used to recompute the guidance law is given by

$$\hat{\mathbf{Y}}(\tau) = \mathbf{Y}(\tau) + \boldsymbol{\upsilon} \tag{35}$$

where $\mathbf{Y} \triangleq \left[\mathbf{r}_1^\top, \, \mathbf{v}_1^\top, \, m_1, \, \mathbf{r}_2^\top, \, \mathbf{v}_2^\top, \, m_2, \, \mathbf{r}_3^\top, \, \mathbf{v}_3^\top, \, m_3\right]^\top$, $\boldsymbol{\upsilon}$ denotes the observation noise, assumed to be zero mean multivariate Gaussian noise, with covariance given by

$$R = \text{diag}\{R_r, R_v, R_m, R_r, R_v, R_m, R_r, R_v, R_m\} \tag{36}$$

where

$$R_r = \begin{bmatrix} \sigma_r^2 & 0 & 0 \\ 0 & \sigma_r^2 & 0 \\ 0 & 0 & \sigma_r^2 \end{bmatrix} \qquad \sigma_r = 5.5 \text{ m} \tag{37}$$

$$R_v = \begin{bmatrix} \sigma_v^2 & 0 & 0 \\ 0 & \sigma_v^2 & 0 \\ 0 & 0 & \sigma_v^2 \end{bmatrix} \qquad \sigma_v = 0.01 \text{ m/s} \tag{38}$$

$$R_m = 5 \cdot 10^{-5} \text{ kg} \tag{39}$$

Finally, the guidance law was recomputed as

$$\mathbf{u}(t; \hat{\mathbf{Y}}(\tau), t_f - \tau) \tag{40}$$

DSM	a [km]	e [-]	i [deg]	Ω [deg]	ω [deg]	f [deg]	m [kg]
1 @ (t_i)	6982.00	0.003500	51.5334	+0.01667	10.0100	50.100	8
2 @ (t_i)	6977.00	0.002500	51.4667	−0.01667	9.9900	49.900	8
3 @ (t_i)	6979.25	0.002375	51.5417	+0.02083	9.9875	49.875	8

Tab. 1: Sample mission specifications. Initial orbital elements for DSM_1 (row 1), DSM_2 (row 2) DSM_3 (row 3).

III.III Numerical Results

The sample case shown in this section is based on the SAMSON Project [16]. A scenario is simulated, considering a cluster of three modules $k = 1, 2, 3$, where the following bounds are assumed for the relative distances: $D_{\min} = 1.0\,\text{km}$ and $D_{\max} = 250\,\text{km}$. The time allowed for the establishment maneuver is 5800 sec. The mission lifetime is assumed to be 1 year. The initial conditions for the modules, after they are released from the launcher, are listed in Tab. , which could represent the launch vehicle dispersion about the nominal injection orbit. Due to the mission specifications, in the SAMSON project there is no specific constraints on the payload orbits. Hence, no specific constraints were imposed for the semimajor axis, eccentricity and inclination of Module 1. Clearly, the analytical development shown in Section III. is still valid, but removing the constrains (10).

The following parameters were assumed: $T_n = 0.080\,\text{N}$ and $\text{I}_{sp} = 60\,\text{s}$, drag coefficient $C_{D_1} = C_{D_2} = C_{D_3} = 2.2$, cross-sectional areas of the satellites $S_1 = S_2 = S_3 = 0.11\,\text{m}^2$, $\Delta t_{12} = 0.1\,\text{s}$, $\Delta\Omega_{12} = 0.05^\circ$ and $\Delta t_{13} = 0.05\,\text{s}$, $\Delta\Omega_{13} = 0.025^\circ$. For the design model, the constant density was assumed as $\rho = 1.137\,10^{-13}\,\text{kg/m}^3$.

Figure 2 shows the results of the obtained guidance law. These results were obtained simulating the maneuver, in an open-loop scheme, in the considered design model. For the following discussion, this case is denominated as case A. Fig. 2(a) illustrates the throttle parameter σ for the 3 modules, the mass histories of the 3 modules, as well as the distances $d_{12}(t)$, $d_{23}(t)$, and $d_{31}(t)$. Fig. 2(b) depicts the semimajor axes $a(t)$, the eccentricities $e(t)$, and the inclinations $i(t)$ of the 3 modules. Figure 3 shows the results of the guidance law, still implemented as open-loop, but simulating a more realistic scenario, including geopotential harmonics up to degree and order 10, and density represented according to the model NRLMSISE−00. Moreover it was assumed that the computation of the maneuver was performed with noisy measurements according to Eq. (35). This case is denominated as case B. Fig. 3(a) illustrates the throttle parameter σ for the 3 modules, the mass histories of the 3 modules, as well as the distances $d_{12}(t)$, $d_{23}(t)$, and $d_{31}(t)$. Fig. 3(b) depicts the semimajor axes $a(t)$, the eccentricities $e(t)$, and the inclinations $i(t)$ of the 3 modules. Figure 4 shows the results of the guidance law, but implemented in a closed-loop scheme according to Eq. (34). The simulated scenario included geopotential harmonics up to degree and order 10, and density represented according to the model NRLMSISE−00. It was assumed that the computation of every maneuver was performed with noisy measurements according to Eq. (35). This case is denominated as case C. Since numerically solving two boundary value problems is not an easy task and demands a considerable computational burden, in this example the maneuvers were recomputed every 24.67 minutes of maneuver time. It is seen that Figs. 2-4 are very similar one to each other. From this observation, one can conclude that the adopted design model was very representative of the maneuver dynamics, and thus adding other perturbations do not affect the maneuver execution. Even adding some measurement noise (case B and C), the solver could still cope with it producing a very similar maneuver to the one of case A.

On the other hand, Figure 5 shows the long-term behavior after the establishment maneuvers of the three cases above described. The notation within Fig. 5 is as follows. "$i-j$, A" indicates $d_{ij}(t)$ obtained by propagating, according to the coasting model, the terminal states resulting from applying the guidance law shown in Fig. 2. In contrast, "$i-j$, B" represents $d_{ij}(t)$ obtained by propagating, according to the coasting model, the terminal states resulting from applying the guidance law shown in Fig. 3. Finally, "$i-j$, C" denotes $d_{ij}(t)$ obtained by propagating, according to the coasting model, the terminal states resulting from applying the guidance law detailed in Fig. 4.

Firstly, it is noticed that in the three cases, the distances are held within the prescribed thresholds. The curves suggest that adding astrodynamical perturbations to the model does not affect significantly the long-term behavior of inter-module distances. Since the obtained post-maneuver behavior for case B is still satisfactory, it is difficult to assess the results of the artificially closed-loop scheme (case C). In other words, it is difficult to say if applying a closed-loop scheme, as the one afore explained, contributes improving the long-term performances of the cluster. Implementing the maneuvers with technological perturbations, namely uncertainties in the thrust level, could be a more challenging scenario which would enable to better assess the contributions of the closed-loop scheme. However, closing the guidance loop as herein suggested may be very difficult for larger level of noises or uncertainties, since it requires to solve at every time τ the two boundary value problem. In conclusion, the cooperative optimal guidance maneuvers herein presented proved to be worth for cluster-establishment (and re-establishment). Therefore, it should be used as reference trajectories to design cluster establishment maneuvers. Yet, the closed-loop approach here suggested should be tested in harder scenarios, and compared in performance terms to other strategies to obtain a closed-

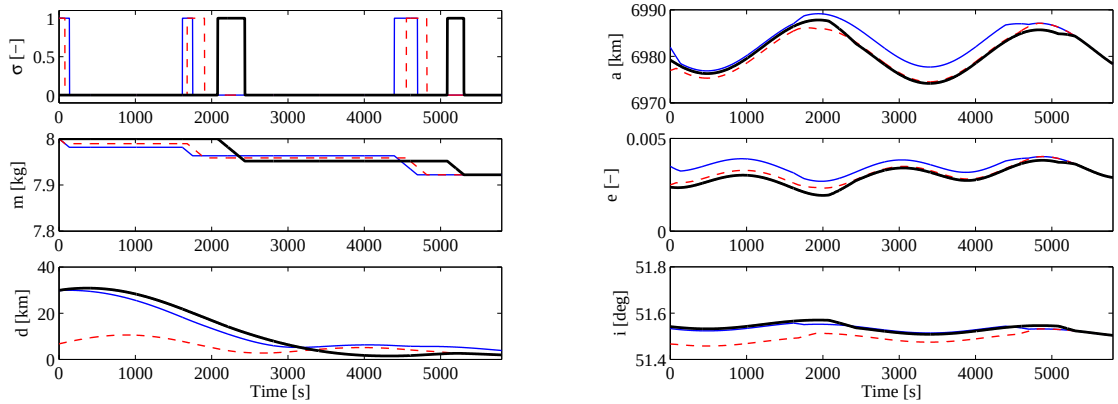

(a) Control variable σ, mass consumption and distances between the modules.

(b) Orbital elements of the modules during the maneuver.

Fig. 2: Establishment maneuver after orbit injection for study case A. Solid line: module DSM_1, dashed line: module DSM_2, bold line: module DSM_3.

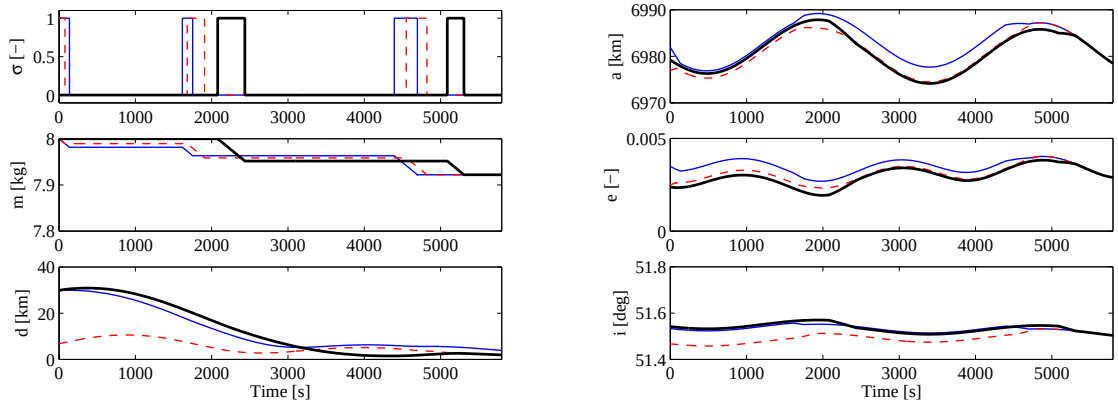

(a) Control variable σ, mass consumption and distances between the modules.

(b) Orbital elements of the modules during the maneuver.

Fig. 3: Establishment maneuver after orbit injection for study case B. Solid line: module DSM_1, dashed line: module DSM_2, bold line: module DSM_3.

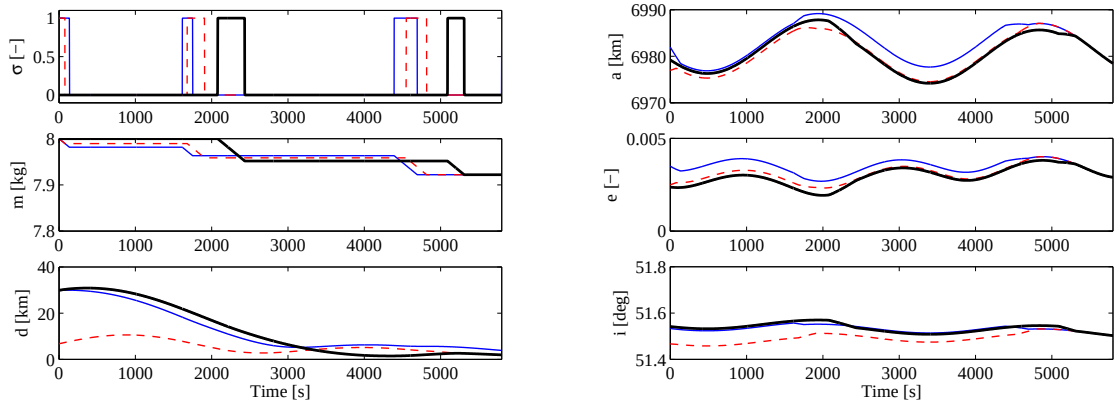

(a) Control variable σ, mass consumption and distances between the modules.

(b) Orbital elements of the modules during the maneuver.

Fig. 4: Establishment maneuver after orbit injection for study case C. Solid line: module DSM_1, dashed line: module DSM_2, bold line: module DSM_3.

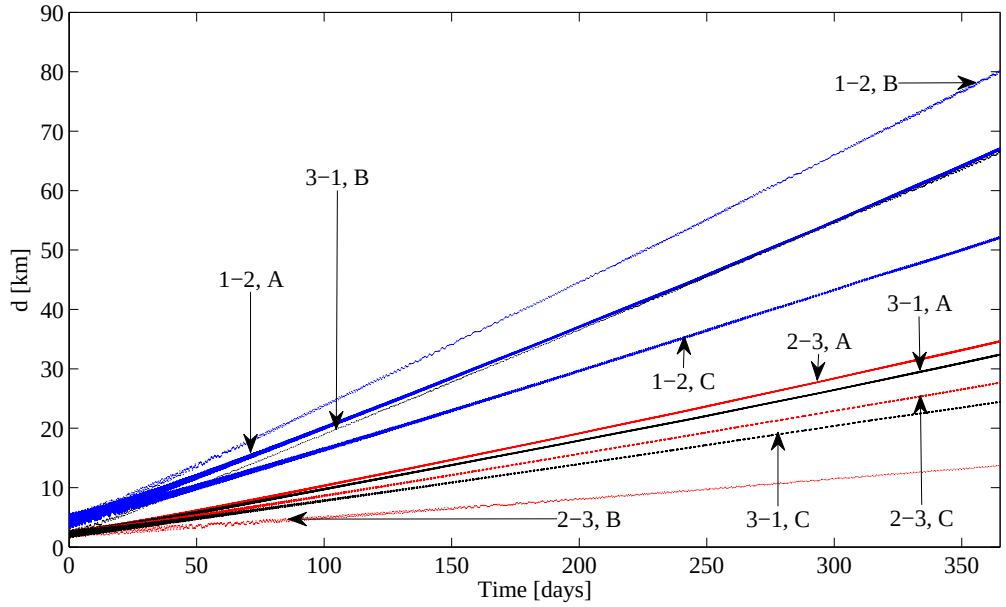

Fig. 5: Establishment maneuver after orbit injection. Solid line: module 1, dashed line: module 2, bold line: module 3.

loop establishment.

III.IV Post-Maneuver Behavior

It is important to mention that constraints (5)-(9), although lead to low rates of drift between distances, they generate a secular mode of the distance behavior which can be downward (the modules get closer one to the other) or upward (the modules get farther one from the other), as shown in Figures 6(a) and 6(b) respectively. Whether the secular behavior of the distances is downward or upward, was observed to be related to $\Delta t_{1k},\ k = 2, 3$ and $\Delta\Omega_{1k},\ k = 2, 3$. If the maneuvers were properly performed, the distance between the modules immediately after the maneuver will be of the order of few kilometers as seen in Figs. 6(a) and 6(b). Therefore, to avoid collision risks, it is preferable that after the maneuver the distances will bear an upward secular behavior, getting farther one from the other. In light of the previous paragraph, it is important to investigate how the secular behavior post-maneuver will be. The following theorem is helpful to understand the secular behavior post-maneuver.

Theorem 1 *For sufficiently small Δt_{1k}, the terminal states given by*

$$\begin{aligned}\mathbf{r}_k(t_f) =& \mathcal{R}(\Delta\Omega_{1k})\left[\mathbf{r}_1(t_f) + \mathbf{v}_1(t_f)\,\Delta t_{1k} - \frac{\mu}{2}\frac{\mathbf{r}_1(t_f)}{\|\mathbf{r}_1(t_f)\|^3}\,\Delta t_{1k}^2\right]\\ \mathbf{v}_k(t_f) =& \mathcal{R}(\Delta\Omega_{1k})\left[\mathbf{v}_1(t_f) - \mu\frac{\mathbf{r}_1(t_f)}{\|\mathbf{r}_1(t_f)\|^3}\,\Delta t_{1k}\right]\end{aligned} \tag{41}$$

yield $a_k(t_f) > a_1(t_f)$.

Proof

The energy equation states

$$\frac{v_1}{2} - \frac{\mu}{r_1} = -\frac{\mu}{2\,a_1} \tag{42}$$

where $v_1 \triangleq \|\mathbf{v}_1(t_f)\|$, $r_1 \triangleq \|\mathbf{r}_1(t_f)\|$, and $a_1 \triangleq a_1(t_f)$. Computing the first-order differential of Eq. (42),

$$v_1\,\mathrm{d}v_1 + \frac{\mu}{r_1^2}\mathrm{d}r_1 = \frac{\mu}{2\,a_1^2}\mathrm{d}a_1 \tag{43}$$

Since $\mu/\left(2\,a_1^2\right) > 0$,

$$\mathrm{sgn}\left(\mathrm{d}a_1\right) = \mathrm{sgn}\left(v_1\,\mathrm{d}v_1 + \frac{\mu}{r_1^2}\mathrm{d}r_1\right) \tag{44}$$

where $\mathrm{d}v_1 = \|v_k(t_f)\| - v_1$, $\mathrm{d}r_1 = \|r_k(t_f)\| - r_1$, and $\mathrm{d}a_1 = a_k(t_f) - a_1(t_f)$. From Eq. (41), $\|v_k(t_f)\|$ can be written as

$$\|v_k(t_f)\| = \sqrt{v_1^2 - \frac{2\mu\,\Delta t_{1k}}{r_1^2}\,v_1\,\cos\gamma + \frac{\mu^2\Delta t_{1k}^2}{r_1^4}} \tag{45}$$

where γ is the flight-direction angle. Eq. (45) can be written as a second order Taylor series about $\Delta t = 0$,

$$\|v_k(t_f)\| \simeq v_1 - \frac{\mu\,\cos\gamma}{r_1^2}\,\Delta t_{1k} + \frac{\Delta t_{1k}^2\mu^2\sin^2\gamma}{2\,v_1\,r_1^4} \tag{46}$$

On the other hand, from Eq. (5), $\|r_k(t_f)\|$ can be written as

$$\|r_k(t_f)\| = \sqrt{\psi} \tag{47}$$

where

$$\begin{aligned}\psi =& r_1^2 + 2\,r_1\,v_1\,\cos\gamma\,\Delta t_{1k} - \frac{\mu}{r_1}\Delta t_{1k}^2\\ &+ v_1^2\,\Delta t_{1k}^2 - \frac{\mu\,v_1\,\cos\gamma\,\Delta t_{1k}^3}{r_1^2} + \frac{\mu^2\Delta t_{1k}^4}{4\,r_1^4}\end{aligned} \tag{48}$$

Eq. (47) can be expressed as a second order Taylor series about $\Delta t = 0$,

$$\|r_k(t_f)\| \simeq r_1 + v1\,\cos\gamma\,\Delta t_{1k} - \frac{\Delta t_{1k}^2}{2}\,\frac{\mu - r_1\,v_1^2\,\sin^2\gamma}{r_1^2} \tag{49}$$

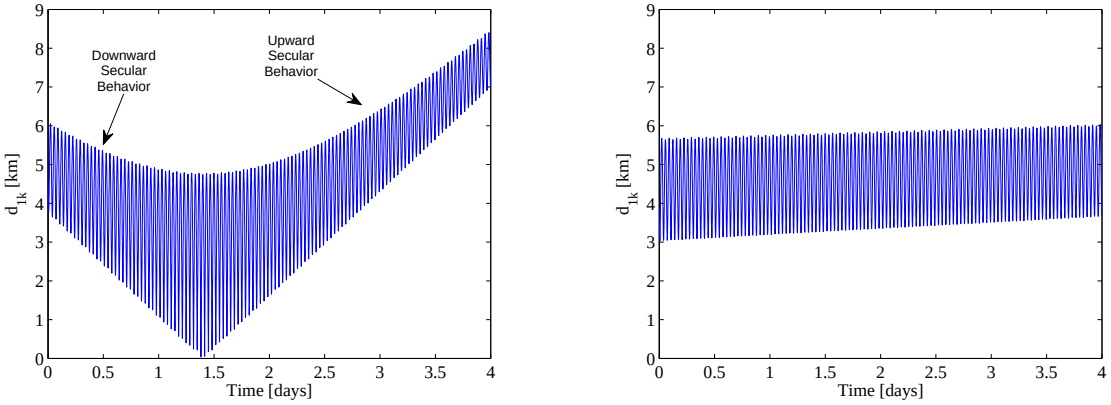

(a) Post-maneuver downward secular behavior.

(b) Post-maneuver upward secular behavior.

Fig. 6: Post-maneuver secular behavior.

Introducing Eqs. (46) and (49) into Eq. (43), and manipulating algebraically yields

$$\frac{\mu}{2\,a_1^2}\mathrm{d}a_1 = -\frac{\mu\Delta t_{1k}^2}{2\,r_1^4}\left(\mu\,\cos^2\gamma - v_1^2\,r_1\,\sin^2\gamma\right) \quad (50)$$

hence,

$$\begin{aligned}\mathrm{sgn}\left(\mathrm{d}a_1\right) &= -\mathrm{sgn}\left(\mu\,\cos^2\gamma - v_1^2\,r_1\,\sin^2\gamma\right)\\ &= -\mathrm{sgn}\left(\mu\,\cos^2\gamma - \frac{h_1^2}{r_1}\right)\\ &= -\mathrm{sgn}\left(\cos^2\gamma - \frac{p_1}{r_1}\right)\end{aligned} \quad (51)$$

where p_1 is the semi-latus rectum.

Defining $\beta \triangleq \cos^2\gamma - \frac{p_1}{r_1}$, it will be determined whether β is positive or negative. To that end, β is written in terms of eccentricity $e_1 \triangleq e_1(t_f)$ and true anomaly $f_1 \triangleq f_1(t_f)$. According to [17],

$$\cos\gamma = \frac{\mu}{h\,v}\,e\,\sin f \quad (52)$$

Introducing Eq. (52) into β, and manipulating

$$\beta = \frac{\mu}{a_1\,\left(1-e_1^2\right)\,v_1^2}\,e_1^2\,\sin^2 f_1 - 1 - e_1\,\cos f_1 \quad (53)$$

From Eq. (42),

$$\frac{1}{v_1^2} = \frac{a_1\,r_1}{\mu\,\left(2\,a_1 - r_1\right)} \quad (54)$$

and introducing Eq. (54) into Eq. (53) yields

$$\beta = \frac{1}{\left(1 + 2\,e_1\,\cos f_1 + e_1^2\right)}\,e_1^2\,\sin^2 f_1 - 1 - e_1\,\cos f_1 \quad (55)$$

Since $1 + 2\,e_1\,\cos f_1 + e_1^2 \geq 1 - 2\,e_1 + e_1^2 = (1-e)^2 > 0$, $\mathrm{sgn}(\beta) = \mathrm{sgn}\left(\xi\right)$ where $\xi \triangleq \beta\,\left(1 + 2\,e_1\,\cos f_1 + e_1^2\right)$. Thus,

$$\xi = -1 - 3\,e_1\,\cos f_1 - e_1^2 - 3\,e_1^2\,\cos^2 f_1 - e_1^3\,\cos f_1 \quad (56)$$

It can be proven that, for eccentricities $e_1 < 0.6812$, ξ will be always negative. To that end, Eq. (56) is differentiated as

$$\frac{\mathrm{d}\xi}{\mathrm{d}\cos f_1} = -3\,e_1 - 6\,e_1^2\,\cos f_1 - e_1^3 \quad (57)$$

from which the maximum is obtained at $\cos f_1 = -\frac{3\,e_1 + e_1^3}{6\,e_1^2}$. To assess that a maximum is obtained, the second derivative is computed

$$\frac{\mathrm{d}^2\xi}{\mathrm{d}(\cos f_1)^2} = -6\,e_1^2 \leq 0^3 \quad (58)$$

The maximum of ξ attains

$$\xi\left(\cos f_1 = -\frac{3\,e_1 + e_1^3}{6\,e_1^2}\right) = -\frac{1}{4} + \frac{1}{2}e_1^2 + \frac{1}{12}e_1^4 \quad (59)$$

In order for $\xi\left(\cos f_1 = -\frac{3\,e_1+e_1^3}{6\,e_1^2}\right)$ to be positive at its maximum, the condition for e_1 is given by $e_1 > \sqrt{2\sqrt{3}-3} \approxeq 0.68125$. In other words, as long as $e_1 < 0.68125$ ξ will be always negative, and so will be β. Therefore, for $e_1 < 0.68$, $\mathrm{sgn}(\mathrm{d}a_1) = -\mathrm{sgn}(\beta) > 0$. For cases in which $e_1 > 0.68125$, one should find the anomalies f_1 at which ξ switches its sign. However, the orbits of interest in this work lie in the region of low eccentricities, $e_1 < 0.1$. The reader should keep in mind that some second order approximations were done, and these conclusions are valid in the range of Δt where the Taylor expansions hold valid. ■

The significance of Theorem 1 can be understood as follows.

For properly small Δt_{1k}, Eqs. (41) yield orbital elements of module 1 very similar to those of module k (excepting the right ascension of the ascending nodes). Since $a_1(t_f) < a_k(t_f)$, according to the first-order mapping between mean and osculating elements presented in Ref. [18], one can assume that $\bar{a}_1(t_f) < \bar{a}_k(t_f)$ will hold, where $\bar{a}$ denotes the mean value of the osculating semimajor axis. Hence, the time that takes module 1 to complete one revolution is shorter than that of k. Therefore, if at $t = t_f$ module 1 is along-track ahead of module k, module 1 will get farther from module k. Conversely, if at $t = t_f$, module 1 is along-track behind module k, it will get closer to it. Figure 7(a) schematically shows module 1 ahead of a module α, and behind a module β.

Assume that for given Δt_{1k_1} and $\Delta\Omega_{1k_1}$, a downward secular behavior is obtained. This module k is represented by the black circle in Fig. 7(b). For the same $\mathbf{r}_1(t_f)$ and

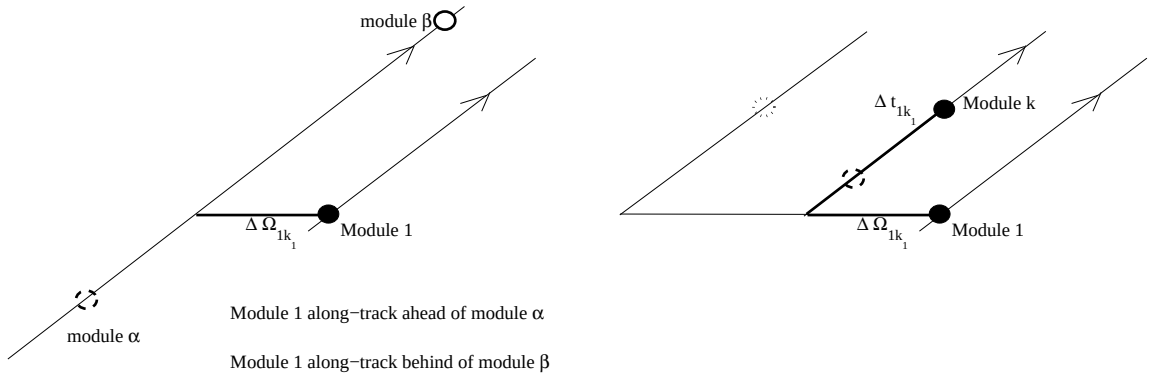

(a) Schematic illustration of module 1 ahead and behind of other modules.

(b) Schematic illustration of the influence of Δt_{1k} and $\Delta\Omega_{1k}$ to shift the modules in the along-track direction.

Fig. 7: Influence of Δt_{1k} and $\Delta\Omega_{1k}$ in shifting the modules in the along-track direction.

$\mathbf{v}_1(t_f)$, reducing to $\Delta t_{1k_2} < \Delta t_{1k_1}$ (dashed circle in Fig. 7(b)) moves module k backward in the along-track direction. Hence, it contributes in obtaining an upward secular behavior of the distances. On the other hand, for the same $\mathbf{r}_1(t_f)$ and $\mathbf{v}_1(t_f)$, keeping Δt_{1k_1} and enlarging $\Delta\Omega_{1k}$ (dotted circle in Fig. 7(b)) moves satellite k backward in the along-track direction for inclinations $0^\circ < i < 90^\circ$, contributing in obtaining an upward secular behavior . Conversely, enlarging $\Delta\Omega_{1k}$ moves satellite k forward in the along-track direction for inclinations $90^\circ < i < 180^\circ$, and thus contributes in obtaining a downward secular behavior.

In order to illustrate these effects, an example of two modules is shown. For a $\Delta\Omega_{1k} = 0.05^\circ$ and $\Delta t_{1k} = 1$ sec, the behavior seen in Fig. 6(a) was obtained. Whereas, keeping $\Delta\Omega = 0.05^\circ$, but reducing Δt_{1k} to $\Delta t_{1k} = 0.1$ sec, the upward secular behavior seen in Fig. 6(b) was obtained.

With respect to the secular component of the distance behavior between modules 2 and 3, a similar argument can be used. According to Eq. (50), it is seen that the larger Δt, the higher da_1, and thus the higher the semimajor axis of the module k. If $\Delta t_{12} \gtrless \Delta t_{13}$, $a_2(t_f) \gtrless a_3(t_f)$, then it is expected that $\bar{a}_2(t_f) \gtrless \bar{a}_3(t_f)$. Therefore, for given Δt_{12} and Δt_{13}, one can exploit $\Delta\Omega_{12}$ and $\Delta\Omega_{13}$ to induce an upward secular behavior of the distance between modules 2 and 3.

IV. CONCLUSION

This work presented optimal guidance laws, which enable establishment and maintenance of a cluster of disaggregated satellite modules during long-term missions. The derived guidance strategies are optimal in the sense of minimizing the fuel consumption of the whole cluster, while balancing the remaining fuel in each module. The guidance strategy was assessed under more realistic astrodynamical models than the adopted design model, and considering possible measurement errors. In these more realistic scenarios it was still seen that the performances of the maneuvers were satisfactory, enabling to hold the cluster for one year with only one maneuver.

On the other hand, an approach was provided that allows to better understand the secular mode of the distance behavior, after the maneuvers. This is meaningful to obtain desired post-maneuver behaviors, when applying the herein developed strategy.

V. ACKNOWLEDGMENTS

This work was supported by the European Research Council Starting Independent Researcher Grant – 278231: Flight Algorithms for Disaggregated Space Architectures (FADER), the Ministry of Science of the State of Israel, and the Technion Graduate Fellowship Program.

Bibliography

[1] O. Brown and P. Eremenko. Fractionated space architectures: A vision for responsive space. In *4th Responsive Space Conference*, 4th Responsive Space Conference, Los Angeles, CA, 2006.

[2] C. Mathieu and L. Weigel. Assessing the fractionated spacecraft concept. In *Space 2006*, Space 2006, San Jose, CA, 2006.

[3] S. R. Vadali, H. Schaub, and K. T. Alfriend. Initial conditions and fuel-optimal control for formation flying of satellites. In *AIAA Guidance, Navigation, and Control Conference and Exhibit*, Portland, OR, 1999.

[4] H. Schaub and K.T. Alfriend. j_2 invariant relative orbits for spacecraft formations. *Celestial Mechanics and Dynamical Astronomy*, 79(2), February 2001.

[5] David Mishne. Formation control of satellites subject to drag variations and J_2 perturbations. *Journal of Guidance, Control and Dynamics*, 27(4):685–692, July-August 2004.

[6] I. Beigelman and P. Gurfil. Optimal fuel-balanced impulsive formationkeeping for perturbed spacecraft orbits. *Journal of Guidance, Control and Dynamics*, 31 (5):1266–1283, September-October 2008.

[7] L. Mazal and P. Gurfil. Cluster flight algorithms for disaggregated satellites. *Journal of Guidance, Control and Dynamics*, 2012, to appear.

[8] M.S. De Queiroz, V. Kapila, and Q. Yan. Adaptive nonlinear control of multiple spacecraft formation flying. *Journal of Guidance, Control, and Dynamics*, 23 (3), 2000.

[9] Z. Wang, F. Khorrami, and W. Grossman. Robust adaptive control of formationkeeping for a pair of satellites. In *American Control Conference, 2000. Proceedings of the 2000*, volume 2, pages 834–838. IEEE, 2000.

[10] D. Izzo and L. Pettazzi. Autonomous and distributed motion planning for satellite swarm. *Journal of Guidance Control and Dynamics*, 30(2):449–459, 2007.

[11] J. Gergaud, T. Haberkorn, et al. Homotopy method for minimum consumption orbit transfer problem. *ESAIM Controle Optimisation et Calcul des Variations*, 12:294, 2006.

[12] T. Guo, F. Jiang, and J. Li. Homotopic approach and pseudospectral method applied jointly to low thrust trajectory optimization. *Acta Astronautica*, 71:38–50, February–March 2012.

[13] L. Mazal, G. Mingotti, and P. Gurfil. Continuous-thrust cooperative guidance law for disaggregated satellites. In *AIAA/AAS Astrodynamics Specialist Conference*, number AIAA-2012-4742, Minneapolis, MN, August 2012.

[14] A.E. Bryson and Y.C. Ho. *Applied Optimal Control: Optimization, Estimation, and Control*. Hemisphere, 1975.

[15] H.P. Geering. *Optimal Control with Engineering Applications*. Springer Verlag, 2007.

[16] P. Gurfil, J. Herscovitz, and M. Pariente. The SAMSON project - cluster flight and geolocation with three autonomous nano-satellites. In *26th AIAA/USU Conference on Small Satellites*, Salt Lake City, UT, USA, August 2012.

[17] R.H. Battin. *An introduction to the mathematics and methods of astrodynamics*. AIAA Education Series, 1999, Chapter 3, pp. 128.

[18] H. Schaub and J.L. Junkins. *Analytical mechanics of space systems*, volume 1. AIAA, 2003, Chapter 14, pp. 731.